Astron. Astrophys. 354, 667–673 (2000)

ASTRONOMY AND ASTROPHYSICS

Theoretical interpretation of the apparent deceleration in the HH 34 superjet

Sylvie Cabrit[1] **and Alejandro Raga**[2]

[1] Observatoire de Paris, DEMIRM, UMR 8540 du CNRS, 61 Avenue de l'Observatoire, 75014 Paris, France
[2] Instituto de Astronomía, UNAM, Ap. 70-264, 04510 D. F., México

Received 31 August 1999 / Accepted 24 November 1999

Abstract. The HH 34 superjet shows a steep velocity decrease (from ~ 500 to ~ 100 km s^{-1}) over a distance of ~ 2 pc on either side of the central source. We explore whether or not this behaviour could be interpreted as evidence for a slow "turning on" of the ejection velocity of the jet, and find that this is indeed possible, but only for an ejection velocity that has had a dramatic growth over the last $\sim 10^4$ yr, and is just about to stabilize within the next 4000 yr. We argue that such a time-variability is somewhat unlikely.

We then explore a second scenario, in which the slowing down of the HH 34 superjet is modeled as the result of the interaction of a fragmented jet with the surrounding environment. We find that for parameters appropriate for HH 34, this model does appear to reproduce the observed slowing down of the superjet in a natural way. We therefore conclude that the kinematical properties of the HH 34 superjet are most likely to be the result of environmental drag on the propagation of individual jet knots, resulting from the fragmentation of a time-variable, precessing jet.

Key words: ISM: jets and outflows – ISM: individual objects: HH 34 – hydrodynamics – stars: formation

1. Introduction

It has recently been discovered that several well-known Herbig-Haro (HH) jets, which have typical lengths of ~ 0.1 pc (see, e. g., Reipurth 1989; Mundt et al. 1987), possess further along their axis a system of more or less aligned bow-shaped knots extending to distances of several parsecs from the exciting source. These so-called "superjets" have been detected in HH 34 (Bally & Devine 1994; Devine et al. 1997; Eislöffel & Mundt 1997), HH 1/2 (Ogura 1995), HH 111 and several other objects (Reipurth et al. 1997; Rosado et al. 1999; Devine et al. 1999a, b).

A particularly detailed study of a superjet is the work on HH 34 carried out by Devine et al. (1997). These authors present both radial velocity and proper motion measurements for 20 knots that show a clear trend of decreasing velocities with increasing distance from the source, with radial velocities dropping from 190 km/s in the first bowshock to 20-50 km/s at distances of 1.5 pc. This apparent deceleration has two possible interpretations:

- that the jet is approximately ballistic, and that the decreasing velocity vs. distance trend is the result of a slow "turning on" of the ejection (i. e., that the ejection velocity has had a monotonic increase over the past $\sim 10^5$ years),
- that we are observing the slowing down of jet material as a result of the drag due to its interaction with the surrounding medium (this latter scenario being favoured by Devine et al. 1997).

Of course, the real situation could also be a combination of these two scenarios.

In the present paper, we first investigate the possibility of modelling the kinematics of the HH 34 superjet as a result of a monotonically increasing ejection velocity (Sect. 2). We then discuss the alternative possibility of explaining the observed kinematics as a result of the interaction of the jet with the surrounding environment in Sect. 3. The relative success of these two models is discussed in Sect. 4. We conclude that the latter scenario is the most likely, and that the distant knots in superjets are probably "old" internal jet working surfaces which are being strongly decelerated by the ram pressure of the ambient medium.

2. The HH 34 superjet as a ballistic jet from a time-dependent source

2.1. The observed kinematics

The HH 34 superjet consists of a number of fragmented working surfaces, which can be modelled as a result of an ejection velocity time variability with a period of ~ 1000-2000 yr (Devine et al. 1997). Fig. 1 plots the velocities of these working surfaces as a function of distance from the source, obtained from the radial velocities and positions measured by Devine et al. (1997). In order to determine spatial velocities, we have not used the measured proper motions, since they have considerably larger errors (Devine et al. 1997). We have instead deprojected the radial velocities and observed positions assuming a constant angle

Send offprint requests to: sylvie.cabrit@obspm.fr

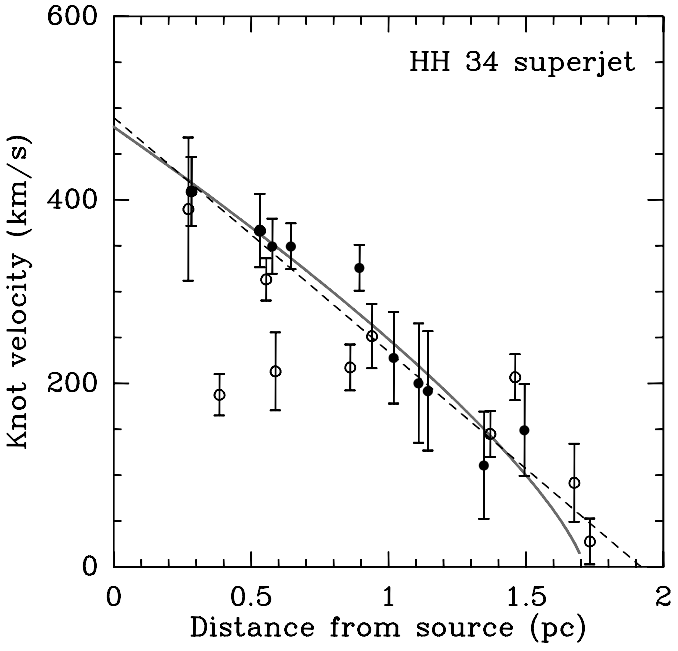

Fig. 1. Spatial velocity vs. distance for the North (filled circles) and South (open circles) knots of the HH 34 superjet system. The radial velocities and positions measured by Devine et al. (1997) have been deprojected assuming a constant angle $\phi = 28°$ to the plane of the sky. The "errorbars" denote the velocity width in each knot. The dashed line shows a linear fit to the data (see Sect. 2.1). The grey curve shows the predicted behaviour for constant mass clumps decelerated by the ambient medium (see Sect. 3).

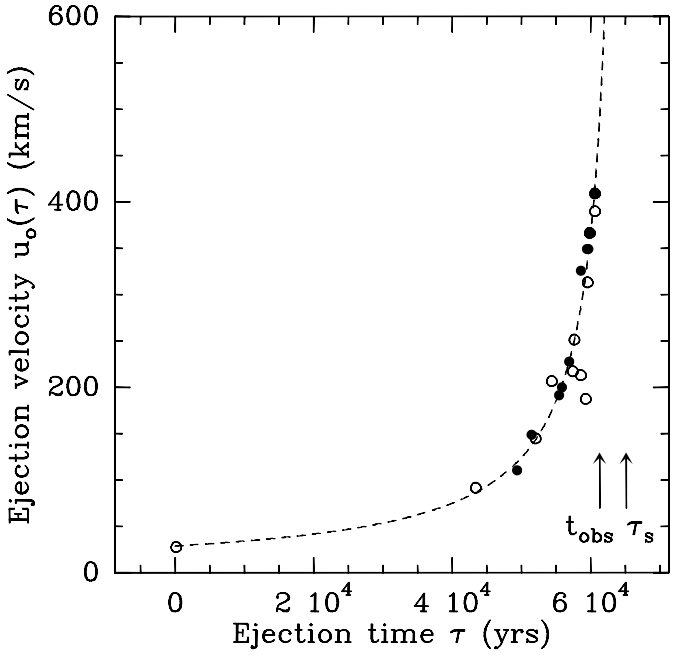

Fig. 2. The reconstructed ejection velocity vs. time dependence for the North (filled circles) and South (open circles) knots of the HH 34 superjet system. The dashed curve shows the velocity law that would reproduce the linear velocity-position trend shown in Fig. 1. The origin of time was set at the ejection time of the farthest knot. Arrows indicate the present time $t_{obs} = 6.1 \times 10^4$ yr and the time at which the velocity law would diverge to infinity, $\tau_s = 6.5 \times 10^4$ yr (see Sect. 2.2).

$\phi = 28°$ between the jet and the plane of the sky (Devine et al. 1997).

As noted by Devine et al. (1997), the knots in the HH 34 superjet clearly appear to "slow down" as a function of distance, in a roughly linear fashion. We have represented in Fig. 1 as a dashed line the best linear fit found by Devine et al. (1997) for the North lobe. The same linear law also reasonably reproduces the average trend in the South lobe (although some knots appear to deviate slightly from this trend). This law has a velocity $v_0 = 490$ km s^{-1} at the source ($x = 0$) and would extrapolate to zero velocity at a distance $x_s = 1.92$ pc. The minimum velocity actually measured in the North lobe of the HH 34 superjet is $v_{1,N} = 110 - 150$ km s^{-1} at $x_{1,N} \sim 1.5$pc, while the South lobe extends somewhat further to $x_{1,S} \sim 1.7$pc and to a lower velocity $v_{1,S} \sim 30 - 90$ km s^{-1}. One thus observes a total velocity range of a factor $v_0/v_{1,N} \sim 5$ in the North lobe, and $v_0/v_{1,S} \sim 10$ in the South lobe.

If the working surfaces in the HH 34 superjet are still contained within the jet beam, their space velocity should reflect some average between the jet velocities just upstream and downstream from the working surface (Raga and Kofman 1992). The apparent "slowing down" of the HH 34 superjet would then indicate that, superimposed on the quasi-periodic variability giving rise to the multiple working surfaces, there is an underlying global trend of decreasing jet speed with distance. We will assume in the following that this global trend is given to a good approximation by the observed decrease of working surface velocity with distance.

The inferred monotonic decrease in jet speed with distance would imply that the jet has been ejected with a monotonically increasing velocity over time. It is possible to reconstruct the past history of the ejection velocity increase necessary to reproduce the present day kinematics of the HH 34 superjet (see Raga et al. 1990): if the jet is free-streaming, the ratio of jet distance to jet velocity at a given position directly corresponds to the time elapsed since that given portion of the jet was ejected from the source (see Eq. 1 of Sect. 2.2). The result of this exercise is shown in Fig. 2.

Fig. 2 shows that a rather steep velocity increase over time is required to reproduce the velocity-position trend in the HH 34 superjet. In Sect. 2.2, we will investigate various functional forms for this velocity increase, and see which properties they must fulfill in order to also reproduce the total velocity range ratio $v_0/v_1 \sim$ 5-10 observed in HH 34.

2.2. The observable velocity range in jets with monotonically increasing ejection velocity vs. time

For a jet with monotonically increasing ejection velocity, the maximum value of the flow velocity v_0 is always encountered at the origin $x = 0$ and corresponds to the ejection velocity at the present time t, while the minimum velocity v_1 is encountered in the material immediately upstream of the leading working

surface, located at a distance x_1 from the source. In order to determine analytically the observable velocity ratio v_0/v_1 we assume that between $x = 0$ and $x = x_1$ we have a free-streaming jet flow, which then satisfies the relation:

$$u(x,t) = \frac{x}{t-\tau} = u_0(\tau)\,, \tag{1}$$

where $u(x,t)$ is the velocity of a jet parcel at a distance x from the source and at time t, τ is the time at which the parcel at (x,t) was ejected from the source, and $u_0(\tau)$ is the time-dependent ejection velocity. The position x and flow velocity $u(x,t)$ are then related at a given time of observation t through the parametrized relationships

$$x = (t-\tau)\; u_0(\tau) \tag{2}$$

$$u(x,t) = u_0(\tau)\,, \tag{3}$$

with τ ranging from 0 to the current time t.

We find that, for a wide class of "not too steep" monotonically increasing functions $u_0(\tau)$ (such as the power-law and exponential functions considered below), the resulting axial velocity vs. position law $u(x,t)$ has an interesting behavior illustrated in the schematic diagram of Fig. 3. Namely, the relationships in Eqs. (2) and (3) admit two "branches" of solutions: A high velocity, physical branch (solid line in Fig. 3) corresponding to jet material that is indeed freely streaming; and a low velocity, unphysical branch (dashed line in Fig. 3) corresponding to slower material ejected early on, that has in fact already been taken over by the faster more recent ejecta and is now piled up at the leading working surface of the jet. The two branches of the solution meet at a distance x_c from the source such that $(dx/du)_{x_c} = 0$. Using Eq. (2), one finds the following conditions on the distance x_c and the corresponding ejection time τ_c:

$$\frac{d\ln u_0}{d\tau}(\tau_c) = \frac{1}{t-\tau_c}\,, \tag{4}$$

$$x_c = u_0(\tau_c)(t-\tau_c)\,. \tag{5}$$

If the inertia of the leading working surface is negligible (i. e., because the shocked material is ejected sideways) and the jet is much denser than the surrounding environment, the position x_1 of the leading working surface will coincide with x_c, and $v_1 = u_0(\tau_c)$. If these conditions are not met, the working surface will have a position $x_1 < x_c$ and v_1 could slightly differ from $u_0(\tau_c)$. In this section we will only consider the simpler, $x_1 = x_c$ equation of motion for the leading working surface. In Sect. 2.3 we will present numerical simulations that take into account the actual propagation of the working surface, showing that our analytical estimate of the velocity range remains essentially valid.

Let us now investigate specific functional forms for $u_0(\tau)$ that follow the behavior illustrated in Fig. 3, and let us determine their corresponding velocity range v_0/v_1. We first consider the case of a power law source variability:

$$u_0(\tau) = a\,\tau^p\,, \tag{6}$$

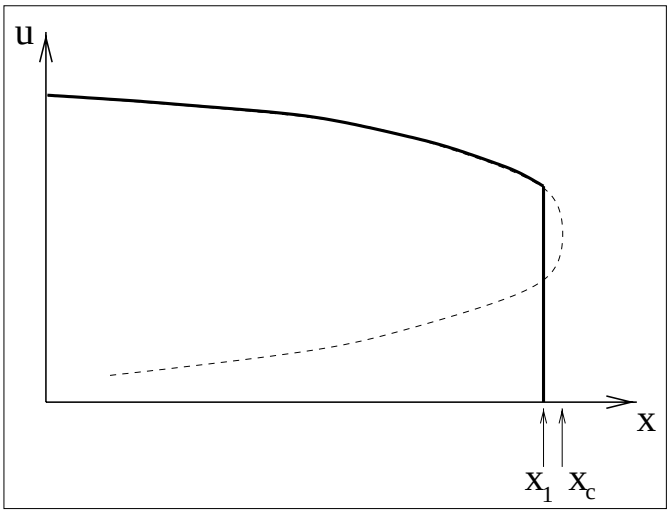

Fig. 3. Schematic diagram of the velocity vs. position for a jet with relatively moderate monotonic increase of ejection velocity over time. The solid curve corresponds to the velocity of the free-streaming jet material, which ends at the position x_1 of the working surface. The full free-streaming solution (including the material that has actually been caught up by the working surface) is given by the curved, solid line, and then continued as a dashed line. The point x_c where $(dx/du) = 0$ determines the lowest possible observable velocity in the jet. The actual position x_1 of the working surface will be somewhat closer to the source (and, hence, the lowest observable velocity will be somewhat higher), but for the case of a massless working surface moving into a low density medium one will have $x_1 \approx x_c$.

with constant a and $p > 0$. From Eq. (4) we obtain:

$$\tau_c = \left(\frac{p}{p+1}\right)\, t\,. \tag{7}$$

We can now calculate the ratio between the maximum and minimum values of the flow velocity (see Fig. 3):

$$\frac{v_0}{v_1} = \frac{u_0(t)}{u_0(\tau_c)} = \left(1+\frac{1}{p}\right)^p\,, \tag{8}$$

which has a value of 2 for $p = 1$, and asymptotically tends to e for $p \to \infty$. Therefore, the $u_0/u_1 \sim 5-10$ ratios obtained for the HH 34 superjet cannot be explained as the result of a power-law increase of ejection velocity with time.

Let us now consider the case of a steeper, exponential velocity increase:

$$u_0(\tau) = a\, e^{\tau/\tau_0}\,, \tag{9}$$

with constant a and τ_0; using Eq. (4), one obtains

$$\tau_c = t - \tau_0\,, \tag{10}$$

and therefore

$$\frac{v_0}{v_1} = \frac{u_0(t)}{u_0(\tau_c)} = e\,, \tag{11}$$

independent of the constants of the exponential time-variability. This again fails to explain the high $v_0/v_1 \sim$ 5-10 values observed in the HH 34 superjet.

From the above results, it is clear that even quite steep dependencies of the ejection velocity with time $u_0(\tau)$ cannot reproduce the wide velocity range observed in the HH 34 superjet. As shown in Fig. 3, all the slow material ejected before the time τ_c has been taken over by faster ejecta and is thus no longer observable. This catching-up process sets a rather low absolute limit to the range of observable velocities in the jet.

There do exist, however, steeper functional forms of $u_0(\tau)$ that can reproduce the observed velocity range. The most natural way to construct such a function is to "invert" the linear velocity vs. position dependence of the HH 34 superjet (see Fig. 1), which passes through a velocity $v_0 = 490$ km s^{-1} at $x = 0$ and is observed to decrease down to a velocity $v_1 = 28$ km s^{-1} at $x = x_1 = 1.73$pc. We will set the origin of time ($\tau = 0$) at the ejection time of this last knot, so that the present time is $t_{obs} = x_1/v_1 = 6.1 \times 10^4$ yr. It is straightforward to show through Eq. (1) that the corresponding source variability has to have the form (illustrated in Fig. 2):

$$u_0(\tau) = \frac{x_s}{\tau_s - \tau} = \frac{v_1}{1 - \tau/\tau_s}\,, \tag{12}$$

with

$$x_s = \frac{x_1}{1 - v_1/v_0}\,, \tag{13}$$

$$\tau_s = \frac{x_1}{v_1(1 - v_1/v_0)}\,. \tag{14}$$

This source variability results in a velocity vs. position dependence at any time t given by

$$u(x,t) = \frac{x_s - x}{\tau_s - t}\,, \tag{15}$$

which at the time of our observation, $t = t_{obs} = x_1/v_1$, coincides with the linear fit to the HH 34 superjet data. In this way we have constructed a functional form for the time-dependent ejection velocity $u_0(\tau)$ (Eqs. 12-14) that produces a jet with a linear position-velocity dependence (Eq. 15) and with a fixed, independently chosen velocity ratio v_0/v_1.

The fundamental reason why this functional form for $u_0(\tau)$ can reproduce any arbitrarily high velocity ratio v_0/v_1 is that there is no "catching up" of the slowest material ejected early on: at any time $t < \tau_s$, the velocity vs. position $u(x,t)$ follows a straight line (see Eq. 15) and (dx/du) is never zero (unlike in Fig. 3). Thus, the full range of ejection velocities, from v_1 at $\tau = 0$ to v_0 at $\tau = t$, remains observable.

Unfortunately, this family of functions also has an undesirable property which makes it not very attractive: In HH 34 where $v_0 = 490$ km s^{-1} and $v_1 = 28$ km s^{-1}, we find $\tau_s = t_{obs}/(1 - v_1/v_0) = 6.5 \times 10^4$ yr, hence $\tau_s - t_{obs} \simeq 4000$ yr. Therefore, we would predict that if the source continues having the same functional form of $u_0(\tau)$ that it had in the past, the ejection velocity should dramatically increase to infinite values during the next 4000 years (see Eq. 12) ! More generally, any functional form of $u_0(\tau)$ that is steep enough at recent times to reproduce the large velocity range in HH 34 will predict a very sharp increase in ejection velocity in a very short time after the present observation.

As HH 34 already has an ejection velocity ~ 490 km s^{-1} which is in the upper part of the typical velocity range for HH jets, it seems unlikely that such a dramatic increase in ejection velocity will actually occur. More probably, the ejection velocity will stabilize or start decreasing again within the next 4000 yr. However, it seems highly suspect that we would be catching HH 34 in such a peculiar stage of its evolution, almost exactly at the moment in which the rapidly increasing ejection velocity vs. time is about to suddenly stabilize (either to a constant value or to a decreasing velocity vs. time trend). This unlikely coincidence might be an argument in favour of the alternative explanation proposed for explaining the kinematical properties of the HH 34 superjet, namely deceleration by the ambient medium (see Sect. 3).

2.3. Numerical simulations

In order to illustrate the validity of our analytical approach, we have computed axisymmetric numerical simulations for two different source time variabilities. Model M1 has a linearly increasing ejection velocity of the form:

$$u_0(\tau) = \left[20 + 320\left(\frac{\tau}{10^4\,\mathrm{yr}}\right)\right]\ \mathrm{km\,s^{-1}}\,. \tag{16}$$

Model M2 has a time-dependent ejection velocity of the form:

$$u_0(\tau) = \frac{82\ \mathrm{km\,s^{-1}}}{1 - (\tau\,/\,2.4 \times 10^4\,\mathrm{yr})}\,, \tag{17}$$

which derives from Eqs. (12-14) using $x_1 = 1.6$pc, $v_1 = 82$km s^{-1}, $v_0 = 490$km s^{-1}, and describes the approximate velocity vs. time behavior deduced for HH 34 for the last 2×10^4 yr (see Figs. 1 and 2).

In both models, the initially neutral jet has an ejection number density $n_j = 300$ cm^{-3}, temperature $T_j = 1000$ K and radius $r_j = 10^{17}$ cm, and moves into a homogeneous, molecular environment of number density (of atomic nuclei) $n_{env} = 10$ cm^{-3} and temperature $T_{env} = 100$ K. These two numerical simulations were carried out with the axisymmetric Coral code (which includes a treatment of several ionic, atomic and molecular species, see Raga et al. 1995, 1997; Mellema et al. 1998), in a 3-level binary adaptive grid with a maximum resolution of 9.77×10^{15} cm.

In Figs. 4 and 5, we show the temperature and molecular hydrogen fraction stratifications that result after $t = 1.3 \times 10^4$ yr and $t = 1.7 \times 10^4$ yr time integrations for models M1 and M2, respectively. In these figures, we also show the axial velocity (as a function of distance from the source) obtained from the numerical simulation and from the analytical model (Eqs. (2) and (3) for model M1, and Eq. (15) for model M2, see Sect. 2.2). We see that the agreement between the analytic and numerical results is in both cases excellent over most of the length of the jet, as the high Mach number simulations indeed have a free-streaming jet beam.

There are, however, evident differences in that in the numerical simulations the working surfaces have not traveled as far from the source as predicted by the analytical models (see

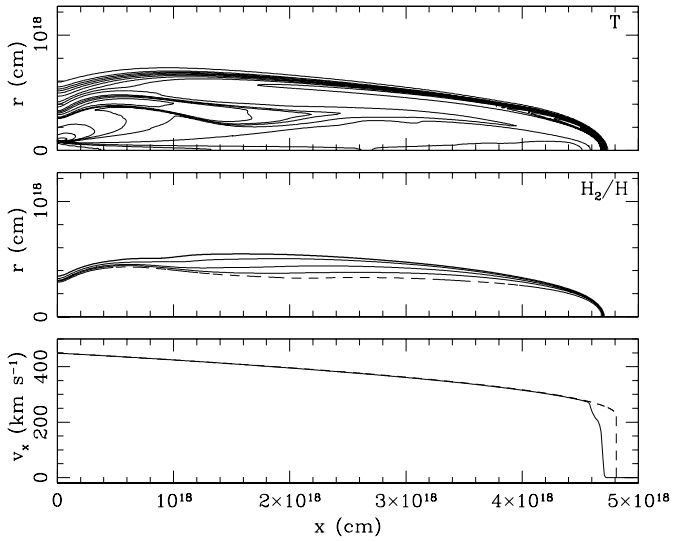

Fig. 4. Model M1 with $u_0(\tau) = \left[20 + 320\,(\tau/10^4\,\mathrm{yr})\right]\ \mathrm{km\,s^{-1}}$ at a time $t = 1.3 \times 10^4$ yr. The top panel shows logarithmic temperature contours, increasing by factors of 2. The middle panel shows linear contours of H_2 to H nuclei abundance ratio, from 0.5 to 0 in steps of 0.1. The bottom panel shows the velocity as a function of distance along the jet axis (solid line) and the analytical prediction from Sect. 2.2 (dashed line).

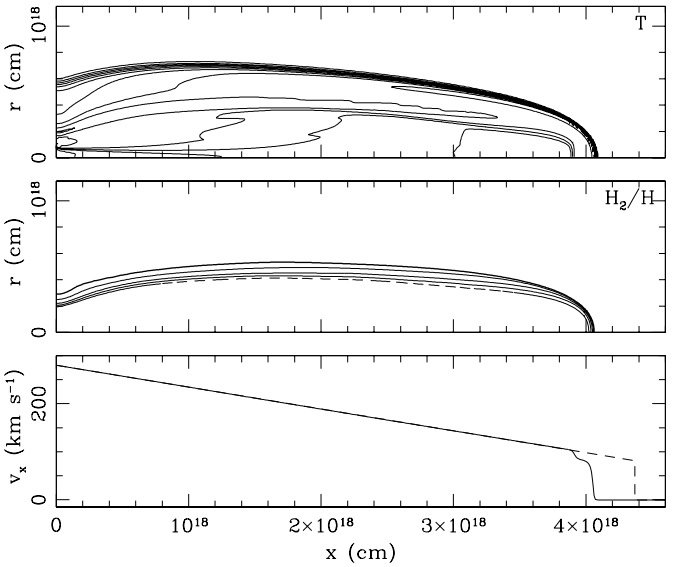

Fig. 5. Same as Fig. 4 for model M2 with $u_0(\tau) = 82\ \mathrm{km\,s^{-1}}/\left[1 - \left(\tau\,/\,2.4 \times 10^4\,\mathrm{yr}\right)\right]$ at time $t = 1.7 \times 10^4$ yr.

Figs. 4 and 5). This is a direct result of the fact that the inertia of the material within the working surface and the ram pressure of the surrounding environment (both of which have been neglected in the analytic model of Sect. 2.2) slow down the motion of the working surface. Yet, the velocity of the shocked material in the leading working surface is very close to the minimum velocity v_1 in the analytical curve (see Figs. 4 and 5), so that the velocity contrast v_0/v_1 is virtually unchanged compared with the corresponding analytical predictions.

3. The HH 34 superjet as braking interstellar bullets

Given the very peculiar phase of evolution that would be required to explain the kinematical properties of the HH 34 superjet as the result of a free-streaming flow from a time-dependent source, it is interesting to consider the alternative possibility of a jet flow which is being slowed down by its interaction with the surrounding environment.

Deceleration could occur in a turbulent jet beam which incorporates matter through a "sideways entrainment" process. This process is in principle related to the details of the turbulent flow within the jet beam itself, but can be theoretically treated with simple, parametrized relations for the entrainment rate. Such an approach has been applied in the past to extragalactic jets by Bicknell (1986), and to HH jets by Raga et al. (1993b).

However, the HH 34 superjet does not appear to have a well defined jet beam. Instead, the images obtained by Devine et al. (1997) show what appear to be highly fragmented working surfaces, which become progressively more misaligned with the HH 34 jet for increasing distances from the jet source. Such a situation is more suggestive of individual knots that travel in scattered directions and directly interact with the surrounding environment.

This scenario is consistent with the model of Raga & Biro (1993a), in which a jet with a quasi-periodic velocity variability and a slow precession fragments into a series of clumps which travel in different directions into the surrounding environment. These high velocity clumps then behave like the "interstellar bullets" proposed by Norman & Silk (1979) for HH objects.

There is of course the question of whether or not these bullets would fragment. Numerical simulations (Nittman et al. 1982; Raga et al. 1998) show a rapid fragmentation of the bullets as soon as they start to break due to the interaction with the surrounding environment. However, the Reynolds number of the simulations is too low by ~ 2 orders of magnitude with respect to the real, astrophysical bullets, so that it is difficult to judge the reliability of the numerical results.

Without considering this complex fragmentation process, we will simply use the plasmon model of De Young & Axford (1967) as revised by Cantó et al. (1998) in order to write an equation of motion for a hypersonic, isothermal clump decelerated by the drag force of the ambient medium:

$$\frac{dv}{dt} = -\left(\frac{\xi \rho_{env} c^4}{M}\right)^{1/3} v^{2/3}\,, \tag{18}$$

where v is the velocity, c the isothermal sound speed and M the (constant) mass of the clump, ρ_{env} is the mass density of the (homogeneous) surrounding environment, and $\xi = 14.0$ is a constant that can be derived from the shape of the plasmon, taking into account the centrifugal pressure of the shocked ambient gas (see Cantó et al. 1998). This equation can be integrated to obtain a deceleration curve:

$$\frac{v(x)}{v_0} = \left(1 - \frac{x}{d_0}\right)^{3/4}\,, \tag{19}$$

where v_0 is the initial velocity of the clump and

$$d_0 = \frac{3}{4}\left(\frac{M v_0^4}{\xi \rho_{env} c^4}\right)^{1/3} = \left[\frac{100\,\mathrm{cm^{-3}}}{n_{env}} \times \frac{M}{10^{-4}\,M_\odot}\right]^{1/3} \times \left[\frac{10\,\mathrm{km\,s^{-1}}}{c} \times \frac{v_0}{480\,\mathrm{km\,s^{-1}}}\right]^{4/3} \times 5.3 \times 10^{18}\mathrm{cm}, \quad (20)$$

with n_{env} being the environmental number density (of atomic nuclei) and $M_\odot$ a solar mass. The scaling parameters in Eq. (20) are chosen to reflect the values expected for the HH 34 superjet, but are of course only indicative. In particular, the clump mass is not well known. The large working surfaces in the HH 34 superjet are thought to be caused by a velocity time-variability of period $\sim$ 2000 yr (Devine et al. 1997). Adopting the jet mass-loss rate of $1.7 \times 10^{-7} M_\odot$ yr^{-1} estimated by Hartigan et al. (1994), the total mass in one working surface should be $\sim 3.4 \times 10^{-4} M_\odot$. Since the working surfaces appear quite fragmented, we have used only one third of this value in Eq. (20) as the typical clump mass.

If we consider v_0 as a free parameter, we find that the knot velocity behavior along the HH 34 superjet can be fit as a deceleration curve (Eq. 19) with $v_0 = 480$ km s^{-1} and $d_0 = 5.3 \times 10^{18}$ cm. This velocity vs. position dependence is shown in Fig. 1 as a thick grey curve. We can see the good agreement that is obtained with the observed velocities. The observed scatter could be reproduced with, for example, small changes of order $\sim$10% in the clump sound speed c.

4. Conclusions

We have attempted to model the slowing down of the HH 34 superjet at large distances from the source as a result of a slow "turning on" of the jet flow. Our analytic and numerical models show that this is only possible if the ejection velocity increased only very slowly over a period of $\sim 5 \times 10^4$ yr, and has then had a very fast increase over the last $\sim 10^4$ yr. Furthermore, in order not to reach unrealistically large values, the jet velocity should stop increasing within the next 4000 yrs. Even though such a time variability is in principle possible, it appears rather unlikely, as we would have to be observing HH 34 at a very peculiar moment in which the time-dependent ejection velocity is showing an anomalous behaviour.

There does appear to be other evidence of an ejection velocity increase as a function of the evolutionary state of the central star, as molecular jets from class 0 sources tend to have lower projected velocities $\sim 50 - 100$ km s^{-1} (e.g. Bachiller et al. 1995; Lefloch et al. 1996; Gueth & Guilloteau 1999) than optical jets from more evolved sources. However, the velocity increase associated with this evolution occurs over longer time periods and does not have the ejection velocity range that would be necessary for explaining the kinematical signature of the HH 34 superjet.

Another possibility is that all of the observed HH 34 superjet could correspond to one period of a quasi-periodic source velocity variability with a period in excess of $\sim 10^5$ years. If this were the case, the reconstruction of the ejection velocity vs. time that we have carried out in Sect. 2.2 (Eq. 12) would still hold. Then, the apparent problem of a recent, very rapid increase in the ejection velocity would still be present.

We have therefore explored a second model, in which a jet fragments and produces "interstellar bullets" which are slowed down through the interaction with the surrounding environment. This model is along the lines of the suggestion of Devine et al. (1997), who propose that the slowing down of the HH 34 jet is due to environmental drag.

Even though the analytical model that we have used for the deceleration of bullets is very simple, a very good agreement is obtained between the predicted and the observed deceleration curves. This agreement suggests that the kinematical properties of the HH 34 superjet could quite naturally be explained as the result of the slowing down of "bullets" as a result of the drag force of the surrounding medium. However, the interaction between a fragmented jet and the environment is a very complex process which is not fully described by our simple, analytic model. Therefore, the present discussion should be considered only as preliminary. Detailed 3-D hydrodynamical simulations of the long-term evolution of precessing, time-variable jets would be necessary to confirm this interpretation.

Acknowledgements. We are grateful to the referee, John Bally, for useful suggestions. The work of A. Raga is supported by the CONACyT grants 26833-E and 27546-E. A. Raga also acknowledges support from the Observatoire de Paris for a visit in which part of this work was carried out.

References

Bachiller R., Guilloteau S., Dutrey A., Planesas P., Martín-Pintado J., 1995, A&A 299, 857
Bally J., Devine D., 1994, ApJ 428, L65
Bicknell G.V., 1986, ApJ 300, 591
Cantó J., Espresate J., Raga A.C., D'Alessio P., 1998, MNRAS 296, 1041
Devine D., Bally J., Reipurth B., Heathcote S., 1997, AJ 114, 2095
Devine D., Bally J., Reipurth B., Shepherd D., Watson A., 1999a, AJ 117, 1919
Devine D., Reipurth B., Bally J., Balonek T.J., 1999b, AJ 117, 2931
De Young D.S., Axford W.I., 1967, Nat 216, 129
Eislöffel J., Mundt R., 1997, AJ 114, 280
Gueth F., Guilloteau S., 1999, A&A 343, 571
Hartigan P., Morse J., Raymond J., 1994, ApJ 436, 125
Lefloch B., Eislöffel J., Lazareff B., 1996, A&A 313, L17
Mellema G., Raga A.C., Cantó J., et al., 1998, A&A 331, 335
Mundt R., Brugel E.W., Bührke T., 1987, ApJ 319, 275
Nittman J., Falle S.A.E.G., Gaskell P., 1982, MNRAS 201, 833
Norman C., Silk J., 1979, ApJ 228, 197
Ogura K., 1995, ApJ 450, L23
Raga A.C., Biro S., 1993a, MNRAS 264, 758
Raga A.C., Cantó J., Binette L., Calvet N., 1990, ApJ 364, 601
Raga A.C., Cantó J., Curiel S., Taylor S., 1998, MNRAS 295, 738
Raga A.C., Cantó J., Calvet N., Rodríguez L.F., Torrelles J.M., 1993b, A&A 276, 539
Raga A.C., Kofman L., 1992, ApJ 386, 222

Raga A.C., Mellema G., Lundqvist P., 1997, ApJS 109, 517
Raga A.C., Taylor S.D., Cabrit S., Biro S., 1995, A&A 296, 833
Reipurth B., 1989, In: Reipurth B. (ed.) Proceedings of the ESO Workshop on Low Mass Star Formation and Pre-main Sequence Objects. ESO, Garching bei München, p. 247
Reipurth B., Bally J., Devine D., 1997, AJ 114, 2708
Rosado M., Raga A.C., Aria L., 1999, AJ 117, 462